Tumor segmentation in lung CT images based on support vector machine and improved level set*

WANG Xiao-peng (王小鹏)**, **ZHANG Wen** (张雯), **and CUI Ying** (崔颖)
School of Electronic and Information Engineering, Lanzhou Jiaotong University, Lanzhou 730070, China

(Received 26 July 2015)

In lung CT images, the edge of a tumor is frequently fuzzy because of the complex relationship between tumors and tissues, especially in cases that the tumor adheres to the chest and lung in the pathology area. This makes the tumor segmentation more difficult. In order to segment tumors in lung CT images accurately, a method based on support vector machine (SVM) and improved level set model is proposed. Firstly, the image is divided into several block units; then the texture, gray and shape features of each block are extracted to construct eigenvector and then the SVM classifier is trained to detect suspicious lung lesion areas; finally, the suspicious edge is extracted as the initial contour after optimizing lesion areas, and the complete tumor segmentation can be obtained by level set model modified with morphological gradient. Experimental results show that this method can efficiently and fast segment the tumors from complex lung CT images with higher accuracy.
Document code: A **Article ID:** 1673-1905(2015)05-0395-6
DOI 10.1007/s11801-015-5148-1

Lung cancer is one of the threats to human life and health, so early detection and diagnosis of lung cancer has got more and more attention. Medical image processing provides a quick and accurate method for tumor identification, diagnosis and treatment, with the tumor segmentation as the key step[1]. In recent years, researchers have proposed many segmentation methods aiming at fast and efficient tumor segmentation, including threshold method, region growing method, fuzzy clustering method (FCM), neural network method, graph cut theory, active contour model and so on[2,3]. Shan et al[4] proposed a region growing method combined with the optimal threshold, finding the seed point with iterative threshold and realizing the image segmentation with region growing. This method needs no artificial marker seed, but the segmentation accuracy of region growing method depends on the seed point, so the result is not accurate for lung tumors with shadow region and inhomogeneous intensity. Fuzzy clustering algorithm[5,6] is more simple and fast, but the selection of initial clustering center is relatively difficult for lung tumors with blur edge or adhesion to tissues. Neural network image segmentation[7] has strong learning ability; however it has high requirements for training samples. If the number of training samples is too small, it often results in over fitting and local optimum, leading to worse generalization performance. Shan et al[8] proposed medical image segmentation based on the assumption that gray level within the tumor region is homogeneous with neural network classifier trained by multidimensional mixed characteristics. Graph cut theory[9] is an energy model of minimizing images, which can take account of both the edge and region information features, and possesses good segmentation effect. Nevertheless, the parameter setting of the energy function requires high level and frequent man-machine interaction, bringing limitations in the fast medical image segmentation. Lan Hong et al[10] adopted the marker controlled watershed algorithm to optimize initial contour curve, and then extracted the target edge by the Snake model. This method is suitable for segmenting large areas with uniform gray distribution.

In lung CT images, some tissues such as vessels and soft tissues have similar gray values to tumor images and adhering tumors. Meanwhile, various sizes and complex environment of lung tumors often present fuzzy edges although their gray values are higher than those of the background of lung region. Aiming at the complex environment between tumors and tissues, we put forward a lung tumor segmentation method based on support vector machine (SVM) and the level set. Firstly, the statistical learning method is used to detect the tumor region, training the classifier in terms of block features of image training sets and taking the texture, gray and shape features as the basis for classifying test samples; and then the level set model modified by morphological gradient is taken to segment the tumor more accurately. The edge

* This work has been supported by the National Natural Science Foundation of China (No.61261029) and Jinchuan Company Research Foundation (No.JCYY2013009).
** E-mail: wangxp1969@sina.com

of suspected lesions is extracted as the initial evolving contour, which can not only eliminate the noise and enhance edge information, but also retain the marginal integrity.

The process is shown in Fig.1, which includes 3 steps:

Step 1: Divide the image into sub blocks with fixed size to test and extract the sub block features;

Step 2: Detect the suspected lesion, training the SVM classifier, inputting the test image and conforming the feature classification;

Step 3: Segment tumors by the improved level set method, optimizing the suspected lesion area and then extracting the edge as the initial contour.

According to the physiological characteristics of lung cancer, the tumor is generally located in the lung, and some special adhering tumors can be connected to the lung area, with erosion of the pleura. In lung cancer CT images, texture, gray scales and shape features are obviously different from those of other tissues, so we use their statistical characteristics to distinguish the tumor and background. In order to accelerate the classification of SVM, a lung CT image is divided into several equal sub blocks. To avoid too many block samples containing both tumors and other tissues, the blocks should not be too large.

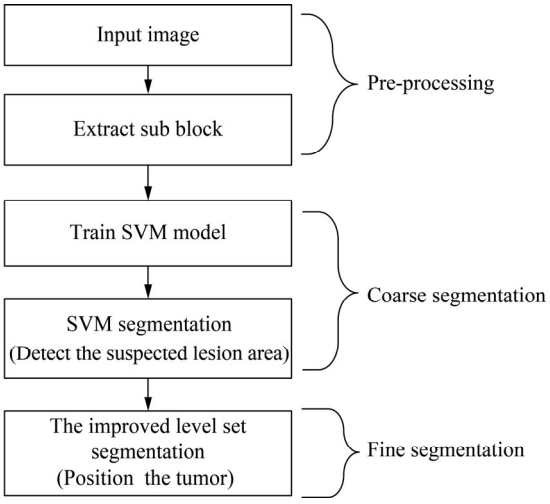

Fig.1 The proposed flowchart

The circularity serves as the shape feature of tumor target in sub blocks, which is defined as:

$$R_{\mathrm{C}} = 2\times\pi\times A / P^2, \tag{1}$$

where $R_{\mathrm{C}} \in [0,1]$ is the circularity; A and P represent the area and perimeter, respectively. When the target shape is close to a circle, R_{C} is approaching 1. The gray feature is averaged to all gray values in the sub blocks, while the texture feature[12] is calculated by the convolution between Gabor filter and sub block in different directions and frequencies.

Assuming the two-dimensional Gabor function $h(x,y)$ is the mother wavelet, Gabor wavelet filter can be obtained through the scale and rotation transformation:

$$\begin{cases} h_{mn}(x,y) = c^{-m}h(x',y'), c>1, m,n\in\mathbf{Z} \\ x' = c^{-m}(x\cos\theta + y\sin\theta) \\ y' = c^{-m}(y\sin\theta - x\cos\theta) \end{cases}, \tag{2}$$

where θ and c^{-m} respectively denote the chief axis direction and scale factor. The direction and scale of the Gabor filter are adjusted by m and n.

By extracting the shape, gray and 16-dimentional texture features (4 scales, 4 directions: 0°, 45°, 90°, 135°), the 18-dimentional eigenvectors are treated as the SVM classifier samples.

SVM is a statistical machine learning method based on Vapnik-Chervonenkis (VC) dimensional theory and the structural risk minimization, and is suitable for classification problems of the finite small samples. SVM has good generalization ability[13,14]. One can select the best compromise between model complexity and learning ability based on the sample information. In the case of small samples, SVM shows advantages in aspects of convergence, training speed and classification accuracy. Since most sample sets existing in original space are linear and inseparable, a nonlinear mapping function $\Phi: R^{\mathrm{d}} \to H$ is required to map the input data to a novel high dimensional space H and establish optimal hyperplane with maximum classification distance, making the sample sets linear and separable. The corresponding discriminant function is:

$$f(x) = \mathrm{sgn}\left\{\sum_{i=1}^{N}\alpha_i^* y_i\left[\varphi(x)\cdot\varphi(x_i)\right] + b^*\right\}, \tag{3}$$

where α_i denotes the Lagrange coefficient, $\alpha_i \geq 0$, i=1,2,3,⋯,n; b^* is the surface offset of optimal classification; $\{(x_i, y_i), i = 1, 2, \cdots N\}$ and $\{(\varphi(x_i), y_i),\ i$=1,2,3,⋯,$N\}$ respectively denote the sample set in R^{d} and H. Here, the kernel function $K(x,y) = \varphi(x)\varphi(y)$ is introduced to abandon the complex high-dimensional computation. The final optimal classification discriminant function is redefined as follows:

$$f(x) = \mathrm{sgn}\left[\sum_{i=1}^{N}\alpha_i^* y_i K(x,x_i) + b^*\right]. \tag{4}$$

The common SVM kernel functions include radial basis function, polynomial function, S function and so on. This paper chooses the Gaussian radial basis function $K(x,x_i) = \exp(-\|x-x_i\|^2 / \delta^2)$ (x_i is the center of the kernel function and δ is the width of the Gaussian kernel) to train SVM classifier, where the penalty factor and kernel parameter[15] are the focus.

SVM classifier model is established by the following steps: select equal number of positive (tumor) and negative (background) values as samples, and their training sets, test sets data and each dimensional feature are respectively normalized to reduce the loss of information. The principal component analysis is employed to fuse

features, reduce the feature dimension and eliminate the relativity among the features. Finally, the cross-validation grid-search method is sequentially used to search the optimal penalty and kernel parameter in large and then small effective ranges to accelerate the classifier.

For each sub block sample unit, the suspected lesion area can be determined and marked by the normalized test sample data classification. Since the sub block is rectangular, most blocks contain both tumor target and non tumor regions which are with similar features to the tumor, especially for the adhering tumor. Generally, lung and tumor are interconnected in lung CT images. For the purpose of extracting the tumor target, we calculate the area of the suspected tumors and compare it with the threshold, remove those areas less than the thresholding, and the rest is the tumor target.

The level set[16] embeds two-dimensional curve of the image space into three-dimensional surface as the zero level set. The curve of zero level set varies with the surface evolution, and the evolution result of the mobile curve surface is determined by the zero level set position. The great advantages of the level set are stability and topological independency, and the topological structure can naturally change during the evolution.

Since there may exist noise and texture details in detected tumors, it is difficult to segment the tumor contour accurately when the level set method is directly used. Therefore, the variable morphological closing operation is adopted to modify the gradient image. In the gradient image, the pixel with high gradient value usually corresponds to the actual contour of the original image, while the noise and details in the target area correspond to the low gradient gray level, which makes it possible that different gradients can employ morphological closing with different structure elements to preserve the contour position and eliminate local minimum noise and details.

The morphological structure element (circular structure element) radius r changes with the gradient l, that is:

$$l \uparrow \Rightarrow r \uparrow . \tag{5}$$

The reason for the use of circular structure elements is that the same distance between each pixel gradient value and its neighborhoods can be held during the gradient modification. The gray level difference between the current pixel and its neighborhood is reflected by the sum of mean square deviation. For example, the pixel (x, y) with 4-connected neighbors, the gradient value and its sum of square deviation of all pixels in the neighborhood is defined as follows:

$$\sigma_l^2 = \frac{1}{d}\{[l(x-1,y-1)-l(x,y)]^2 + [l(x-1,y+1)-l(x,y)]^2 + [l(x+1,y-1)-l(x,y)]^2 + [l(x+1,y+1)-l(x,y)]^2\}, \tag{6}$$

where d is the distance between the current pixel and target pixel, while $1/d$ is the weighting coefficient; σ_C^2 and $l(x, y)$ denote the square deviation and gradient value, respectively.

Eq.(5) indicates that the gradient level l is a decreasing function of the structure element radius r. In order to describe the quantitative relationship between r and l, a structure elements matrix $\boldsymbol{R}(x, y)$ is constructed with the same size of the gradient image, in which each point denotes the corresponding modified size of structure element for the gradient image. The quantitative relationship between r and l is calculated by the following equation, i.e.,

$$r(x,y) = R_{\max} \sin\left\{\frac{\pi}{2}[1-\alpha\times\sigma_C^2(x,y)]\right\}, (0<\alpha<1), \tag{7}$$

where α denotes the regulative factor, and $r(x,y)$ is the size of structure element. $R_{\max}$ is the maximum radius of the structure element.

The modified image is the layer contour after the morphological closing operation with different structure element radii for different layers:

$$g_m(x,y) = g_d(x,y) \bullet \boldsymbol{R}(x,y) , \tag{8}$$

where $g_d(x,y)$ is the morphological gradient image.

In the level set segmentation, if the contour of modified rectangle block sample is viewed as a planar closed curve L, the curve can be impliedly expressed as an equivalence curve which has the same value of a 3D continuous function $\phi(x,y,t)$ at a certain moment. Let $\phi(x,y,t)$ be the level set function, the sign distance function is defined as:

$$\phi(x,t) = 0 = \pm s , \tag{9}$$

where s is the shortest distance from point x to the initial closed curve $L(t=0)$, whose sign depends on the point x inside or outside the curve. Generally, inside is positive and outside is negative.

Introduce energy function as follows:

$$E(\phi) = \mu P(\phi) + E_{g,\lambda,\nu}(\phi) , \tag{10}$$

where μ denotes the internal energy weight. The internal energy function is defined as:

$$P(\phi) = \iint_{\Omega} \frac{1}{2}(|\nabla\phi - 1|)^2 \mathrm{d}x\mathrm{d}y , \tag{11}$$

where Ω is the image domain. The internal energy function is mainly used to restrain over deformation in evaluation, decide whether $\phi(x,y,t)$ is closed to the sign distance function, avoid the level set function repeated initialization and reduce the computational complexity.

The definition of external energy function is:

$$E_{g,\lambda,\nu}(\phi) = \lambda A_g(\phi) + \nu B_g(\phi) , \tag{12}$$

where ν is a constant (if the target is inside the curve, $\nu > 0$, ensuring the curve to shrink inward to the object

edge; otherwise, $v<0$, outward to the object edge); λ ($\lambda>0$) is a coefficient. $A_g(\phi)$ and $B_g(\phi)$ are used to calculate the length of closed curve and speed up the curve evolution, respectively. They are respectively defined as follows:

$$A_g(\phi)=\iint_{\Omega} g\delta(\phi)\left|\nabla\phi\right|\mathrm{d}x\mathrm{d}y \ , \tag{13}$$

$$B_g(\phi)=\iint_{\Omega} gH(-\phi)\mathrm{d}x\mathrm{d}y \ , \tag{14}$$

where δ and H denote the Dirac function and the Heaviside function, respectively, and g is the edge detection function defined as:

$$g=\left|\nabla G_\sigma * g_{\mathrm{d}}(x,y)\right|=\frac{1}{1+\left|\nabla G_\sigma * g_{\mathrm{d}}(x,y)\right|^2} \ , \tag{15}$$

where G_σ is the Gaussian filter. The external function can make the curve infinitely approach the target edge.

When the zero level set function evolves to the stable state, it satisfies the following condition:

$$\frac{\partial\phi}{\partial t}=0=-\frac{\partial E}{\partial\phi} \ . \tag{16}$$

Therefore, the level set evolution can be rewritten as:

$$\frac{\partial\phi}{\partial t}=-\frac{\partial E}{\partial\phi}=$$

$$\mu[\nabla\phi-\nabla(\frac{\nabla\phi}{|\nabla\phi|})]+\lambda\delta(\phi)\nabla(g\frac{\nabla\phi}{|\nabla\phi|})+vg\delta(\phi) \ . \tag{17}$$

The level set function is updated in the two-dimensional plane without calculating the evolution result during the curve evolution, and the zero level position obtained is the final tumor segmentation contour.

After the improved level set segmentation, the complete and accurate lung tumor contour can be achieved.

In this section, 193 pieces of clinical medicine CT lung tumor images are selected to test the performance of the proposed method. All simulations are implemented in MATLAB, and the resolution of test images is 1 920×1 200. 123 images are training sets and 70 images are for testing, in which there are 18 images with adhering tumor.

Fig.2 shows the lung benign tumor segmentation results using different methods. Fig.2(a) is the original image, Fig.2(b) is the result of suspected lesions detected by SVM (C=90, γ=25), and it is obvious that speckle noise and other formation exist. Fig.2(c) is the gradient image after the area thresholding (132 pixels), and it can be seen that other small tissues around the tumor are eliminated. Fig.2(d) is the result of Fig.2(c) after gradient modification ($R_{\max}$=16, α=0.06). Fig.2(e) shows the final segmentation result using the proposed method with the level set model (μ=0.1, λ=5, v=1.5) on the basis of Fig.2(d). Fig.2(f) is the superposition of the proposed segmentation result and the original image, and it can be seen that the noise details and non-target areas in the detection region are eliminated, while a complete tumor contour is preserved. Fig.2(g) and (h) are the segmentation results by optimal thresholding region growing and traditional level set model, respectively, and they are both under segmentation and there exists tumor contour bias. Compared with the expert manual outline as shown in Fig.2(i), the proposed method has higher positioning accuracy in the lung tumor segmentation.

Fig.3(a) is a CT tumor image with lung and tumor adhesion. Fig.3(b) shows the tumor lesion area detected by SVM (C=97, γ=22), indicating that the tumor features (shape, texture and gray) determined by training sample sets have better ability to separate tumor from lung edge tissue. Fig.3(c) demonstrates the result after the local optimization in improved level set (μ=0.1, λ=5, v=1.5, $R_{\max}$=15, α=0.1), and it is almost the same as Fig.3(f). In contrast, Fig.3(d) and Fig.3(e) are under segmentation, where part of the tumor is outside the segmented contour since the gray value discrimination of target is affected by the fuzzy edge of adhering tumor.

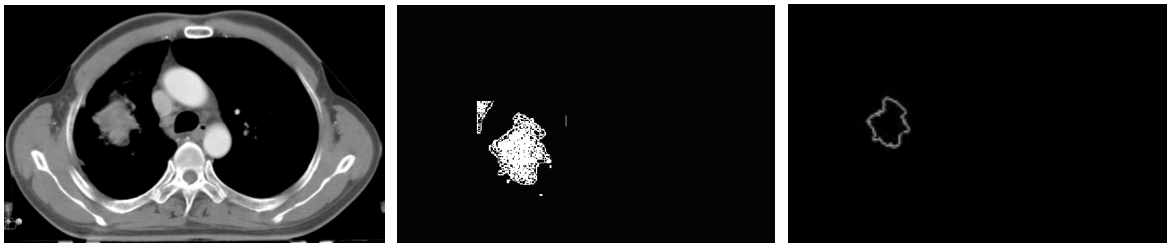

(a) The original image (b) SVM detection result (amplification) (c) Gradient image after area thresholding

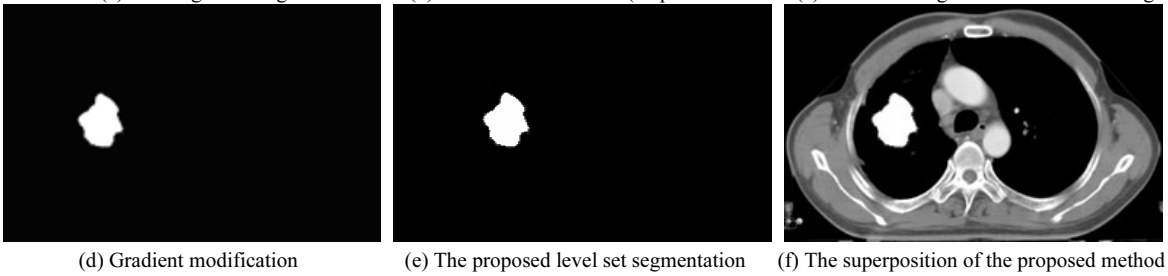

(d) Gradient modification (e) The proposed level set segmentation (f) The superposition of the proposed method

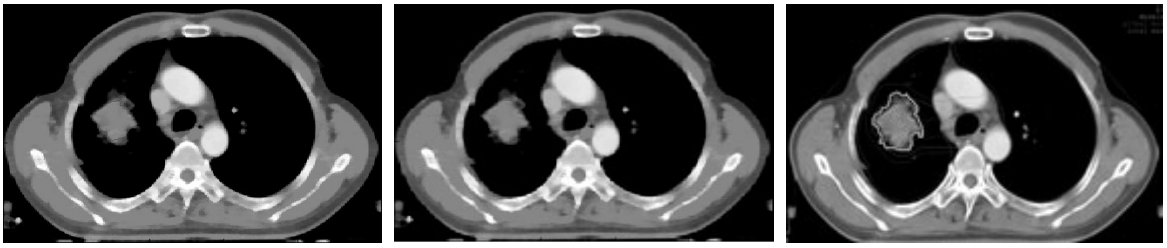

(g) Region growing with optimal thresholding (h) The traditional level set segmentation (i) The expert manual outline result

Fig.2 Benign tumor segmentation results in lung CT image with different methods

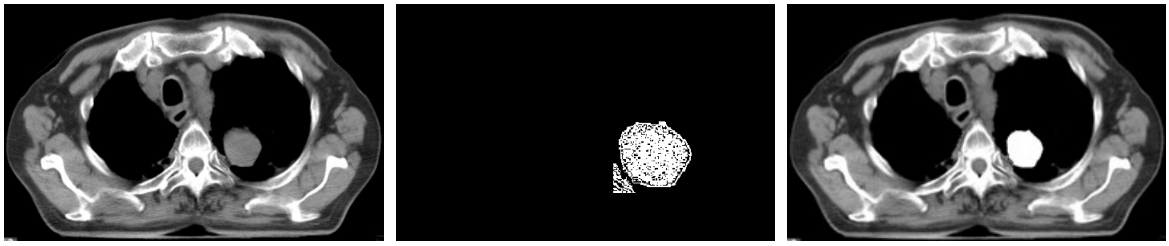

(a) The original image (b) SVM detection result (amplification) (c) The proposed segmentation

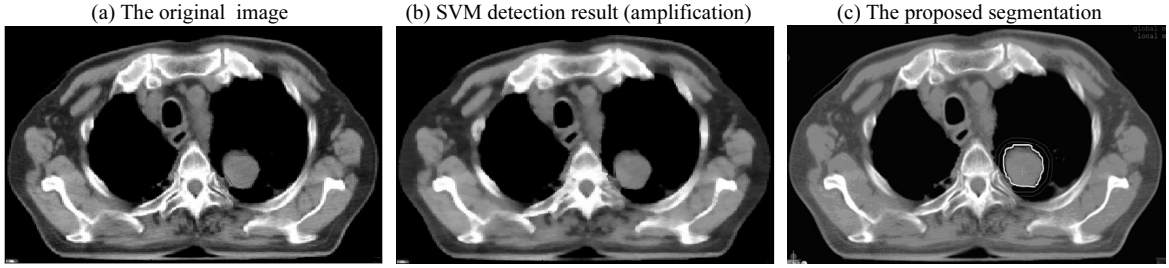

(d) Region growing with optimal thresholding (e) The traditional level set segmentation (f) The expert manual outline result

Fig.3 Adhesion tumor segmentation results in lung CT image with different methods

For the quantitative evaluation of the proposed segmentation, the actual segmentation area and expert outline are overlapped, and the fault tolerant rate and accuracy rate are introduced as the evaluation parameters. The fault tolerant rate is defined as:

$$F = [N - (N_{\mathrm{h}} \cap N_{\mathrm{a}})] / N , \tag{18}$$

where N_{h} and N_{a} are pixel numbers of real tumor outlined by an expert and segmentation result methods, respectively; $N_{\mathrm{h}} \cap N_{\mathrm{a}}$ denotes the overlapping pixel number of the area marked by experts and segmentation method. N is the total pixel number of the tumor.

The accuracy rate P is defined as:

$$P = [N_{\mathrm{h}} \cap N_{\mathrm{a}}] / N_{\mathrm{h}} . \tag{19}$$

The smaller F and the larger P indicate that the segmentation result is closer to the manual area, and its accuracy is higher. Tab.1 gives the data comparison of different segmentation methods for Fig.2 and Fig.3, which shows that the proposed method has smaller fault tolerance rate and higher accuracy than the region growing and traditional level set methods.

Tab.2 shows the computational complexity comparison between the traditional level set and the proposed method. In contrast, the proposed method avoids the time-consuming process of dealing with all the pixels of the whole image in the traditional level set, and greatly reduces the calculation time.

Tab.1 Comparison of different segmentation methods

Tissue	Index (%)	Region growing	Traditional level set	The proposed method
Benign tumor	F	11.31	13.72	6.23
	P	91.18	90.83	95.32
Adhesion tumor	F	10.68	12.06	5.63
	P	93.16	92.43	96.12

Tab.2 Comparison of computation complexity

Tissue	Index	Traditional level set	The proposed method
Benign tumor	Iteration times	135	20
	Accuracy rate (%)	88.59	94.67
Adhesion tumor	Iteration times	150	20
	Accuracy rate (%)	91.73	96.07

A lung tumor segmentation method based on SVM and improved level set is proposed. The shape, gray level and texture features of lung tumor are available for training samples, SVM classifier is employed to detect suspected tumor area, area thresholding is adopted to exclude non-tumor, and the level set after gradient modifi-

cation is used to realize lung tumor segmentation. Experimental results show that this method can fast and accurately segment benign tumors with uneven gray or fuzzy edge and malignant adhering tumors. But when the tumor and surrounding tissue are completely infiltrated, tumor features and details may be relatively weak, so further researches are needed in the feature extraction with improved SVM model to improve the segmentation accuracy.

References

[1] LARTIZIEN C, MARACHE F S and PROST R, IEEE Trans. Nucl. Sci **59**, 102 (2012).

[2] LIN Y and TIAN J, International Journal of Pattern Recognition and Artificial Intelligence **6**, 192 (2002). (in Chinese)

[3] DUNCAN J S and AVACHE N, IEEE Transactions on Medical Imaging **33**, 85 (2000).

[4] SHAN J, CHENG H D and Wang Y X, Proceedings of the 19th IEEE International Conference on Pattern Recognition, 1 (2008).

[5] LI Xuchao, LIU Haikuan, WANG Fei and BAI Chunyan, Journal of Image and Graphics **17**, 447 (2012). (in Chinese)

[6] Liu G, Zhao Z and Zhang Y, IEEE Journals & Magazines **12**, 1770 (2015).

[7] CHANG C Y, HONG Y C, CHUNG P C and TSENG C H, IEEE Computational Intelligence Magazine **6**, 43 (2011).

[8] SHAN J, WANG Y X and Cheng H D, Proceedings of the 17th IEEE International Conference on Image Processing, 1713 (2010).

[9] Jung T H, Choi S W and Ko K S, Electronics Letters, 2010.

[10] LAN Hong and ZHANG Lu, Journal of Image and Graphics **17**, 873 (2012). (in Chinese)

[11] Sulaiman S N and Isa N A M, IEEE Transactions on Consumer Electronics **56**, 2661 (2010).

[12] FARROKHINA F and JAIN A K, IEEE Computer Society Conference on Computer Vision and Pattern Recognition, 364 (1991).

[13] MOON P and SPENCER D E, Journal of the Optical Society of America **34**, 234 (1944).

[14] Liu X and Tang J, IEEE Systems Journal **8**, 910 (2014).

[15] Lin K P and Chen M S, IEEE Transactions on Knowledge & Data Engineering **23**, 1704 (2010).

[16] Liu Yugang and Yu Yizhou, IEEE Transactions on Visualization & Computer Graphics **18**, 202 (2012).